THE JOURNAL OF PHYSICAL CHEMISTRY B

Article

pubs.acs.org/JPCB

Electrostatics and Charge Regulation in Polyelectrolyte Multilayered Assembly

Andrey G. Cherstvy*

Institute for Physics & Astronomy, University of Potsdam, 14476 Potsdam-Golm, Germany

ABSTRACT: We examine the implications of electrostatic interactions on formation of polyelectrolyte multilayers, in application to field-effect based biosensors for label-free detection of charged macromolecules. We present a quantitative model to describe the experimental potentiometric observations and discuss its possibilities and limitations for detection of polyelectrolyte adsorption. We examine the influence of the ionic strength and pH on the sensor response upon polyelectrolyte layer-by-layer formation. The magnitude of potential oscillations on the sensor−electrolyte interface predicted upon repetitive adsorption charge-alternating polymers agrees satisfactorily with experimental results. The model accounts for different screening by mobile ions in electrolyte and inside tightly interdigitated multilayered structure. In particular, we show that sensors' potential oscillations are larger and more persistent at lower salt conditions, while they decay faster with the number of layers at higher salt conditions, in agreement with experiments. The effects of polyelectrolyte layer thickness, substrate potential, and charge regulation on the sensor surface triggered by layer-by-layer deposition are also analyzed.

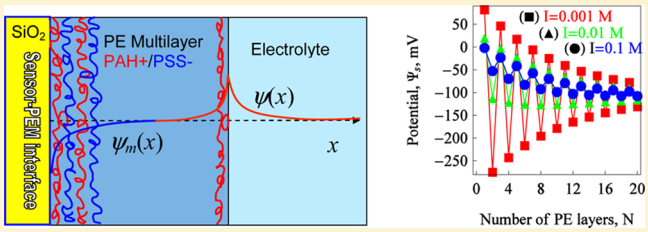

1. INTRODUCTION

Semiconductor field-effect devices (FED) are nowadays some basic elements of electrochemical and biological label-free sensors.[1−3] They are promising tools in particular for detecting pH values, ion concentrations, some enzymatic reactions, and action potentials of living cells. The detection of molecular interactions and charges at solid−liquid interfaces is of great interest for a wide variety of applications, ranging from lens coatings, biomedical implants, and drug carriers to biosensors such as DNA arrays and protein chips. Recently, a considerable effort has been devoted to a label-free electronic detection of charged biomolecules, including DNA and proteins, by FEDs via intrinsic charge.[4−9] The binding of charged macromolecules alters the surface potential at the gate of FED devices and thus measurably alters their operating characteristics.

The quantitative understanding of counterion-mediated screening and effects of charged macromolecules displaced from the sensor surface on electrostatic (ES) detection of molecular charges still poses some challenges (see, e.g., ref 10). FEDs do measure the charge of surface-adsorbed molecules, but counterion condensation can reduce the expected signals, especially at high-salt conditions[11,12] (a physiological solution contains ∼0.10−0.15 M of 1:1 salt). Existing theoretical models offer different mechanisms of charge detection and sometimes have problems with description of relatively large sensor signals observed. Recent experiments with capacitive electrolyte-insulator-semiconductor sensors[13] and silicon-on-insulator thin-film resistors as transducers[14] have demonstrated the possibilities of the FED platform for detection of layer-by-layer polyelectrolyte (PE) adsorption.

Typical PE multilayers (PEMs) are formed, as pioneered by Decher,[15−17] by alternating adsorption of charge-alternating PEs onto interfaces.[18−20] Nowadays, de novo PEM structures are used for a number of industrial applications, i.e., lens coating, food preservation films, anticorrosion films, antireflective coatings, and various biosensor-oriented applications (to enhance measured signals). The formation of hollow PEM capsids can be used, e.g., for drug delivery and colloidal coatings. Programmable PEM formation is governed by polycation−polyanion ES complexation[21,22] and entropy increase due to "evaporation" of counterions bound beforehand on PEs. The latter is akin to the complex formation between DNA and cationic lipid membranes.[23,24] The relative contribution of each of these complexation mechanisms varies with the PE linear charge density ρ and adsorption conditions.

To be ES stable, PEMs should be overall nearly charge-neutral. This is achieved via PE layer charge compensation by the oppositely charged PE layer or by mobile counterions from solution. The former mechanism of *intrinsic* charge neutralization is relevant at low salt.[25] With addition of salt to the outer solution, the PEMs typically swell, the salt ions penetrate inside the layers, and compensate the PE charge *extrinsically*. After PEM preparation, being exposed to salty water, the PEMs swell as well, particularly if they contain weakly charged PEs (does not hold for PSS/PAH). The linear vs exponential growth of the PEM thickness with the number of adsorbed layers N[19,26] is often realized for intrinsic and extrinsic charge neutralization, respectively. Typically, the PE chains with higher ρ form denser and thinner PEMs,[27−29] while loosely looped PE structures are more common for PEMs of weakly charged PEs. In particular,

Received: March 11, 2014
Revised: April 11, 2014
Published: April 11, 2014

the PEM thickness grows as a square root of ionic strength at low salt[30] and scales linearly with ionic strength at high salt (0.5−3 M of NaCl).[17,27] As free ions from solution penetrate PEMs at high salt, PE−PE ES attraction gets progressively screened yielding less dense, floppier complexes. Also, as the PE ES persistence length decreases with [salt], the formation of more extended loops/tails in adsorbed PE layers is possible, whereas at low salinity PEs are relatively stiff and form dense layers. Typical thickness of a PE layer is ca. 0.5−5 nm, with the number of PE layers typically N = 10−100. Very stable PAH/PSS PEMs show nearly linear PEM thickness growth with N, as we assume in the model below.

The effects of a number of environmental factors and experimental parameters, such as pH level, [salt], type of ions, temperature, PE hydration levels, PEM dielectric permittivity, counterion condensation,[31] and ionization equilibrium of PEs and of supporting surfaces,[32,33] onto PEM thickness and growth mechanism have been examined experimentally.[34−40] The formation of PEMs has been studied by theoretical[41−45] and computational approaches of different levels of sophistication.[46−49] In particular, a theoretical description of ES and ionic effects on PEM formation based on a capacitor model and Debye−Hückel theory was suggested in ref 14. It was applied for quantitative analysis of the measured response of FEDs functionalized with the standard PSS/PAH PEMs. The capacitor model proposed assumed different structures of PEs inside PEMs, both well-separated PE layers and fully interdigitated. The linear ES model was shown to give the same results in these two situations indicating that internal charge distribution inside PEMs is of secondary importance for the measured sensor potential. Using the Born ES self-energy, the ion partitioning and dielectric constant of PSS/PAH PEMs were enumerated in ref 14. The surface charge density of adsorbed PAH layers was predicted to be σ = 20 mC/m^2 at 50 mM of salt. We use below a similar ES model of interdigitated PE layers to describe the potential oscillations on the sensor−electrolyte surface upon adsorption of charge-alternating PEs.

The PEM formation by partially charged PDADMAC/PSS was performed in ref 59. It was shown that PE overcharging does not occur; instead, PDADMAC layers exactly compensate the charge on the previous PSS layer. At pH = 7.5 and 50 mM of NaCl the charge of SiO_2 was estimated as −7 mC/m^2. It was shown that there exists a critical ρ of PDADMAC below which no PE adsorption and regular PEM formation takes place. Based on the capacitor model, the [salt] was computed inside PAH/PSS PEMs to be 0.9 mM (the Debye screening length of λ_D = 6 nm), considerably larger than the salt amount in PDADMAC/PSS of 0.02 mM (λ_D = 33 nm).[59] These differences were partially attributed to different dielectric constants ε_m inside PEMs, 30 and 19 correspondingly, and thus to a larger Born ES self-energy penalty for ions to enter PDADMAC/PSS PEMs.

The optimization of the operation principles for detection of charged molecules by FEDs was described in ref 50, i.e., in applications to pH and [salt] sensor sensitivity. The model of the double-layer capacitance and the Grahame equation for coupling surface charge and potential were utilized. The response of the sensor surface to the acid−base equilibrium calculated[50] provided the analytical expressions for surface potential and its sensitivity to the amount of charged species adsorbed.

The PEM structures often cease forming at large [salt] >2−3 M of NaCl. Experiments indicate the existence of a critical charge density of the supporting interface σ_s required for PEM formation,[51] and there exists a critical PE charge density ρ below which no PEMs are formed.[29] These observations are qualitatively consistent with the predictions of the theory of PE adsorption onto oppositely charged surfaces,[52] including low-dielectric interfaces.[53] In particular, in low-salt limit the PE layer thickness was predicted to grow with the reciprocal Debye length, $d \propto \kappa$.[42] The critical σ_s to trigger PE adsorption at low salt was shown to grow as $\sigma_s \propto \kappa^3$ (see eq 25 in ref 54 and eq 7 in ref 42). The dependence of PE layer thickness d on σ_s predicted from the critical PE-adsorption theory is $d \propto (\sigma_s\rho)^{-1/3}$.[54] Note that the thickness of real PEMs exhibits a much stronger dependence on ρ (see, e.g., PDAC−PVTAC PEM data[29]).

Recently, in close collaboration with experimentalists, the author studied the formation of PEMs and presented some theoretical results to describe the observed sensor potential variations.[55] In ref 55, the response of a capacitive sensor consisting of p-Si-SiO_2 structure with a self-assembled PEM of cationic PAH and anionic PSS PEs was investigated by constant-capacitance method at varying κ. The effect of PE layer number N and polarity on the sensor potential shifts has been studied. Also, the layer thickness, wettability, and surface morphology of the adsorbed PE layers were examined by water contact-angle procedure, ellipsometry, and AFM imaging. The reader is referred to ref 55 for more details on the setup, the measurement procedure, and PE properties.

We developed in ref 55 a theoretical model accounting for screening effects, to explain the sensor signal generation upon PEM formation, with the potential jumps in the range of $\Delta\Psi$ ~10−100 mV, depending on conditions and PE layer number N. A distinct decrease in the amplitude of $\Delta\Psi$ with N for PEMs in unbuffered solutions was observed for up to N = 18.[55] These potential oscillations decay with PEM thickness, particularly as it exceeds the screening length inside PEMs, $1/\kappa_m$. Potential variations are more pronounced and extend to larger N for denser PEMs at low [salt], v.gr. 0.001 M vs 0.01 and 0.1 M of NaCl in the buffer.[55] At low salt, however, the potential decay is less reproducible because of the nonideal, strongly patterned structure of adsorbed PEs (partially due to strong ES attraction and nonequilibrium adsorption conditions).

The depletion of free ions inside PEMs and quite immobilized PE charges result in much longer screening lengths inside the film as compared to free solution, cf. Figure 4 below. The charge of terminating PE layer thus "propagates" toward the sensor surface. For 0.01 and 0.1 M of NaCl, the potential variations are reproducible and the length-scale of potential decay can be determined; see Figure 4. Sensor potential oscillations with pH-buffer were shown to be smaller,[57] indicating that the effect measured is due partially to ion redistribution in PEMs affecting PE ionization equilibrium in a varying pH environment,[58] as well as due to direct ES influence of the terminating PE layer.

In this paper, we develop this ES model in further detail to examine the effects of experimentally relevant parameters (e.g., [salt], PE layer thickness, surface charge). In addition, we investigate the implications of the charge regulation on the surface and the linear vs nonlinear ES theories. We first present the ES model of potential distribution in PEMs deposited on a charged sensor surface immersed in electrolyte. We compute the ES potential zigzag oscillations upon PEM formation, for varying model parameters. Then, we examine the effects of the nonlinear vs linear ES theory and charge regulation taking place

dx.doi.org/10.1021/jp502460v | J. Phys. Chem. B 2014, 118, 4552−4560

on the PEM-supporting interface. Finally, we discuss some open questions regarding the sensor response upon PEM formation.

2. POTENTIAL DISTRIBUTION INSIDE PEMS

a. Linear ES Model. To describe the potential variations monitored on the sensor surface in experiments, we use the Debye−Hückel equation for the dimensionless ES potential $\psi = e\varphi/(k_BT)$ inside PEM and outside in solution, namely, $d^2\psi(x)/dx^2 = \kappa^2\psi(x)$. We consider the medium inside PEM as fully charge-compensated dielectric of thickness x_m with some concentration of mobile ions. We suppose that the alternating PE layers inside the PEM compensate one another intrinsically and form a structureless medium we can describe on a coarse-grained mean-field level (neglecting PE molecular details and charge neutralization features). The reciprocal Debye lengths inside and outside PEM are κ_m and κ, respectively, while the dielectric constants are ε_m and ε. The screening length is expressed via the ionic strength of aqueous electrolyte I (in M) as $1/\kappa \approx 3\ \text{Å}/(I(M))^{1/2}$.

The general solution of the linear Poisson−Boltzmann equation inside PEM is the combination of two exponents, $\psi_m(x) = \alpha e^{-\kappa_m x} + \beta e^{+\kappa_m x}$, while outside PEM the potential decays as $\psi(x) = \gamma e^{-\kappa x}$; see Figure 1. To find α, β, and γ, we use three boundary conditions for the potential and its derivative. On the sensor surface we have $\varepsilon_m\psi_m'(0) = 4\pi l_B\varepsilon/S_s$, where $\sigma_s = -e_0/S_s$ is the negative charge density (assumed potential-independent here) and S_s is the surface area per one unit positive charge e_0. On the terminating Nth PE layer, the conditions are $\varepsilon\psi'(x_m) - \varepsilon_m\psi_m'(x_m) = (-1)^N 4\pi l_B\varepsilon/S$ and $\psi_m(x_m) = \psi(x_m)$, with $\sigma = e_0/S$ being the surface charge density of the PE layer. In the model, this charge density is of the same magnitude for positively and negatively charged PE layers (not a bad assumption for PAH/PSS). The term $(-1)^N\sigma$ accounts for the change in sign of the last PE layer. So, the slope of the initial ES potential decay at $x = x_m$ scales with σ, while potential derivative at the sensor surface scales with σ_s. Here and below, $l_B = e_0^2/(\varepsilon k_BT) \approx 7$ Å denotes the Bjerrum length in aqueous solution at room temperature T. The value N is odd for positively charged and even for negatively charged terminating PE layers. As the silicon oxide surface acquires a negative charge at the experimental pH = 5−7,[55] the first PE layer adsorbed is a positive PAH layer. The thickness of an adsorbed PE layer is d (set independent of the charge density), i.e., the PEM thickness is $x_m = Nd$. Resolving the boundary conditions for unknown α, β, and γ, we get

$$\alpha = -2\pi l_B\frac{\varepsilon}{\varepsilon_m\kappa_m}\left[(-1)^N\frac{1}{S} + \left(\frac{\varepsilon\kappa}{\varepsilon_m\kappa_m} + 1\right)\frac{e^{\kappa_m x_m}}{S_s}\right]\left[\frac{\varepsilon\kappa}{\varepsilon_m\kappa_m}\cosh(\kappa_m x_m) + \sinh(\kappa_m x_m)\right]^{-1}$$

$$\beta = \alpha + \frac{4\pi l_B\varepsilon}{\varepsilon_m\kappa_m S_s}$$

and

$$\gamma = e^{\kappa x_m}(\alpha e^{-\kappa_m x_m} + \beta e^{+\kappa_m x_m})$$

that enables us to restore the ES potential distribution. The potential on the sensor surface (in mV), $\psi_s[\text{mV}] = 25\psi_m(0)$, is also recovered. Upon adsorption of the Nth PE layer onto PEM with $(N-1)$ PE layers, the potential on the sensor−electrolyte interface changes by $\Delta\psi_N[\text{mV}] = 25[\psi_m(0,N) - \psi_m(0,N-1)]$.

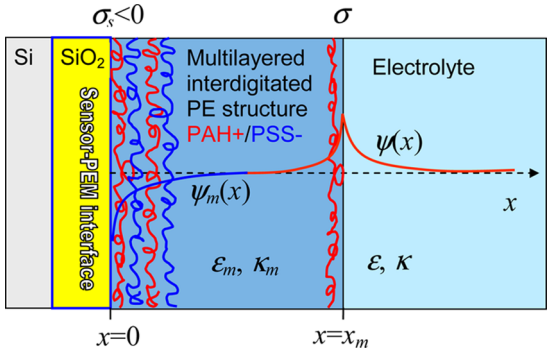

Figure 1. Typical ES potential distribution for positively charged outermost PE layer and negatively charged sensor surface. For the screening lengths inside PEM $1/\kappa_m$ comparable to PEM thickness x_m, the potential variation from the terminal PE layer and sensor surface overlap inside PEM. In contrast, for strong screening when $1/\kappa_m \ll x_m$, the potential variations inside PEM take place only close to $x = 0$ and $x = x_m$ charged boundaries.

b. Main Results. Potential distributions inside and outside PEMs obtained from this model are plotted in Figure 2 for varying layer numbers N, external salinity, and PEM dielectric permittivity. The value of PEM internal ionic strength of 0.001 M used in Figures 2 and 3 is in agreement with experimental data (see also Figure 4). The model results shown in Figures 2a

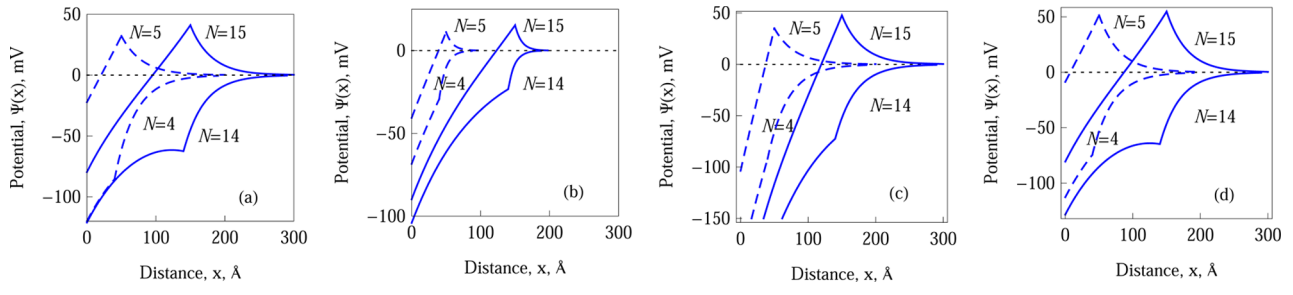

Figure 2. ES potential distribution inside and outside the PEM for $N = 4$, 14 (the last layer is negatively charged (PSS)) and $N = 5$, 15 (the terminal layer is positively charged (PAH)). Parameters for all plots: the surface charge density of the PE layer is $\sigma = e_0/1000$ Å^2, the inverse screening length inside PEM is $\kappa_m = (0.001)^{1/2}/3$ Å, PE layer thickness is $d = 10$ Å, the electrolyte permittivity is $\varepsilon = 80$, and (a) $\varepsilon_m = 80$, $\kappa = (0.01)^{1/2}/3$ Å, $\sigma_s = -e_0/2000$ Å^2; (b) $\varepsilon_m = 80$, $\kappa = (0.1)^{1/2}/3$ Å, $\sigma_s = -e_0/2000$ Å^2; (c) $\varepsilon_m = 30$, $\kappa = (0.01)^{1/2}/3$ Å, $\sigma_s = -e_0/2000$ Å^2; and (d) $\varepsilon_m = 30$, $\kappa = (0.01)^{1/2}/3$ Å, $\sigma_s = -e_0/5000$ Å^2.

dx.doi.org/10.1021/jp502460v | J. Phys. Chem. B 2014, 118, 4552−4560

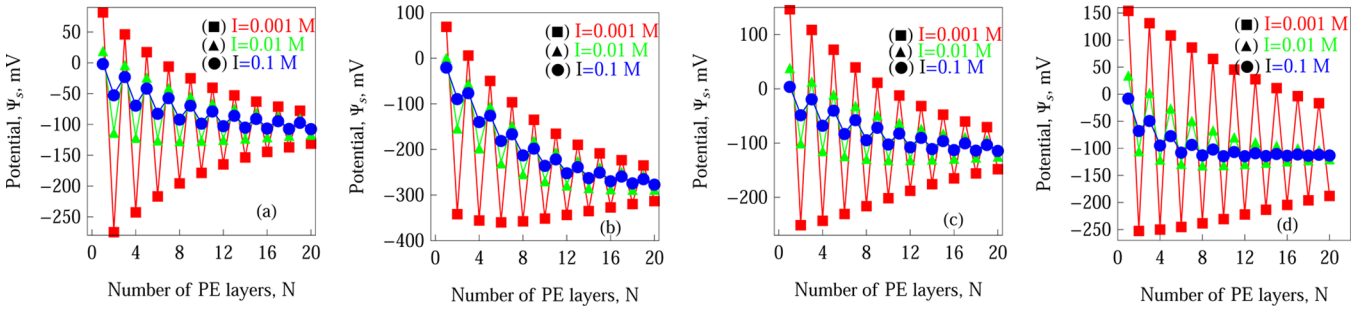

Figure 3. ES potential variations on the sensor surface upon repetitive adsorption of "model" PAH+ layers (N is odd) and PSS- layers (N is even) PE layers. Parameters are the same as in Figure 2 and (a) $\varepsilon_m = 80$, $d = 10$ Å, $\sigma_s = -e_0/2000$ Å^2; (b) $\varepsilon_m = 30$, $d = 10$ Å, $\sigma_s = -e_0/2000$ Å^2; (c) $\varepsilon_m = 30$, $d = 10$ Å, $\sigma_s = -e_0/5000$ Å^2; and (d) $\varepsilon_m = 30$, $d = 6$ Å at 0.001 M, $d = 13$ Å at 0.01 M, $d = 20$ Å at 0.1 M of outer salt, $\sigma_s = -e_0/5000$ Å^2.

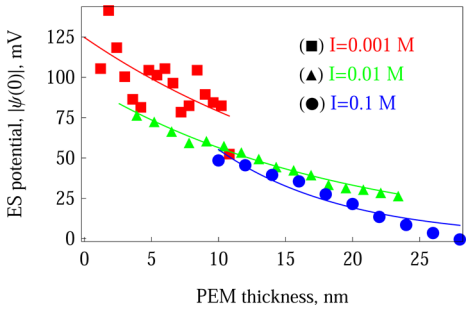

Figure 4. Exponential fits to the magnitude of ES potential oscillations measured experimentally (Figure 6 in ref 55 and Figure 5.13 in ref 56) at varying solution salinities, as indicated in the plot. The PE layer thicknesses used are the same as in Figure 3d. Note considerably more irregular variations of the sensor potential at low [salt] (red squares).

and 3a were presented already in ref 55. We find that as N increases, the potential variation $\Delta\psi_N$ becomes smaller: compare the two dashed vs two solid curves in Figure 2a. These variations on the sensor surface stem from partially screened ES influence of the last PE layer. Eventually, as N grows, the influence of the last layer on the detecting surface is mostly screened by the PEM interior. As the outer [salt] grows, the decay of $\Delta\psi_N$ with the layer number N for the same PEM thickness is faster: compare Figure 2a and b. So, we find that smaller ionic strengths of electrolyte result in larger ES potential values on the PEM−electrolyte interface, in agreement with the experiments. If the PEM dielectric permittivity assumes smaller values, in agreement with experimental observations, the ES potential values on the sensor surface at $x = 0$ are much larger (see Figure 2c). The surface potential values get diminished again if weaker sensor charge density σ_s is used (compare Figure 2c and d), because within this linear ES model the potential magnitude due to PE adsorption scales linearly with σ.

In addition, we observe that larger negative sensor charge density σ_s shift of the sensor potential $\psi_m(0)$ after adsorption of many PE layers to more negative values $\bar{\Psi}$ given by $\bar{\Psi} = -25(4\pi l_B/S_s\kappa_m)(\varepsilon/\varepsilon_m)$ mV. This makes $\Delta\psi_N$ oscillations upon repetitive PE adsorption asymmetric with respect to $\psi = 0$ (see Figure 3). For instance, the value of $\bar{\Psi}$ for the parameters of Figure 2a is −104 mV (it is on the order of ES potential on the surface of bare DNA without condensed counterions).

As a model for PAH/PSS PEMs, zigzag potential oscillations on the sensor surface upon adsorption of positively and negatively charged PEs predicted are shown in Figure 3. The potential $\psi_m(0)$ is more positive upon PAH adsorption and more negative when the last PE layer is PSS. The influence of the charge of this terminating PE layer "propagates" toward the sensor surface. We obtain that for longer Debye lengths λ_D the amplitude of potential oscillations is larger and the potential value reaching the sensor surface decays slower with the number of layers N. For ionic strength of 0.001 M inside PEM, as chosen in Figures 2 and 3, the potential variations and their decay length are qualitatively similar to the experimental trends of Figure 9 in ref 55. Naturally, for shorter $1/\kappa_m$ the ES effects of the last PE layer are screened more strongly and $\Delta\psi_N$ decays more rapidly with PEM thickness (not shown).

We show in Figure 3b the potential oscillations when the dielectric permittivity of PEMs is set smaller, i.e., $\varepsilon_m = 30$ instead of 80 as in Figure 3a ($\bar{\Psi} \approx -278$ mV in Figure 3b as compared to $\bar{\Psi} \approx -104$ mV in Figure 3a). These smaller ε_m values are in agreement with experiments[59] and reflect smaller fraction of free water molecules in densely compressed PEMs. We find that at smaller ε_m the potential oscillations acquire some additional asymmetry because the ES potential $\bar{\Psi}$ for large N reaches more negative values. The behavior for the same low $\varepsilon_m = 30$ but much weaker sensor charge densities is illustrated in Figure 3c ($\bar{\Psi} \approx -111$ mV in this case).

In Figure 3d we examine the situation when PE layer thickness gets smaller at lower [salt], being caused by a stronger ES complexation of PEs inside PEM. Namely, in agreement with experiments,[55] we use for PE layer thickness $d = 6$, 13, and 20 Å for the solution ionic strengths of 0.001, 0.01, and 0.1 M, respectively. We observe that, as compared to the situation of $d = 10$ Å and otherwise identical parameters in Figure 3c, for the PE layer thickness varying as set above, the potential oscillations are more persistent with N at low salt and decay more rapidly with N at high salt. This is attributable to varying thicknesses of PEM structures at different salinities. Note also that the magnitude of potential oscillations about $\bar{\Psi}$ scale with the charge density of the terminating PE layer in this linear ES model.

Potential oscillations presented in Figure 3 are to be compared with the experimentally measured potential shifts based on the constant-capacitance scheme,[55] as presented in Figure 4. Here, we do not try to fit the experimental data of Figure 6 in ref 55 via adjusting the often poorly known and system-specific parameters inside PEMs such as κ_m and ε_m values (it can easily be done).

c. Parameters and Approximations. Typical values for the PE and sensor charge densities ($\sigma = e_0/1000$ Å^2 and $\sigma_s = -e_0/2000$ Å^2) chosen in Figures 2 and 3 are close to those estimated for PAH/PSS PEMs on SiO_2 at pH = 7.5 studied in ref 59. For the pure SiO_2 surface the value of $\sigma_s = -e_0/2300$ Å^2

dx.doi.org/10.1021/jp502460v | J. Phys. Chem. B 2014, 118, 4552−4560

or −7 mC/m^2 was obtained, while for adsorbed PAH+ layers $\sigma = e_0/800$ Å^2[59] and for adsorbed PSS layers $\sigma \approx -e_0/1200$ Å^2.[14,59] At pH = 7.5 the charge density of SiO_2 surface was estimated at −7 mC/m^2, based on the measurements of surface potential difference $\delta\psi = 4\pi l_B S_S^{-1} (3/(I_1)^{1/2} - 3/(I_2)^{1/2}) \approx 9$ mV for two ionic strengths, $I_1 = 0.05$ and $I_2 = 0.5$ M, and provided that the dielectric constant near the SiO_2 surface in PEMs is ∼80.[59] Note that the estimates for SiO_2 charge density can depend on the surface preparation method and experimental conditions.

We use the linear Poisson−Boltzmann equation that can *strongly overestimate* the ES potential near highly charged surfaces with $|\psi(0)| \gg 25$ mV. The qualitative tendencies extracted from the Debye−Hückel model are expected, however, to be correct, likewise for a number of highly charged PE systems; see, e.g., ref 60. We checked that for ES potentials $|\psi| < 25-50$ mV in PEM structures, both the linear and nonlinear Poisson−Boltzmann theory predict quite close sensor potential oscillations upon PEM formation (see Figure 6). We are interested here in general trends rather than in absolute ψ values: the asymmetry of potential oscillations with respect to the sensor surface potential, the decay length of potential oscillations with the PEM thickness, and the effects of dielectric constant value inside PEM, for experimentally relevant parameter values. In the linear model, the magnitude of ES potentials is scalable with surface charge densities, so one can in principle get satisfactory small potentials $|\psi| < 25$ mV just by reducing the corresponding σ and σ_s in the model or adding more salt into PEM, whereas the trends obtained in Figure 3 remain mainly the same.

We use the dielectric constants of 80 and 30 inside PEMs, as experimental data on this issue are quite contradictory. In refs 14,59, ε_m for PSS/PAH PEMs was estimated from the Born ES self-energy calculations. For 0.05 and 0.5 M of NaCl the values $\varepsilon_m = 30$ and $\varepsilon_m = 21$ were obtained, respectively. It was argued that these different ε_m can originate from a different degree of water immobilization (water ordering and binding by densely complexed PEs). The use of $\varepsilon_m = 80$ enables us to neglect the Born ES self-energy emerging upon immersing a charged object from aqueous solution into a medium with different ε. We use very low values of ionic strengths inside PEMs, ∼0.001 M, consistent with experimental estimates for PSS/PAH PEMs.[59] The concentrations of mobile ions inside PEMs can be 10−1000 times smaller than in bulk electrolyte. Namely, the ions surrounding PEs in solution are no longer needed inside PEMs when oppositely charged PEs compensate their charges intrinsically. Because of a long Debye length inside PEMs, the adsorption of the last PE layer triggers the redistribution of ions over the whole PEM reaching the sensor surface. Similar ion redistribution effects also occur upon detection of DNA hybridization in dense DNA arrays at low salt.[12]

The relation between salinities inside PEMs and in outer solution is not a well settled subject, both experimentally and theoretically. In Figure 4 we fit the magnitude of ES potential zigzagging $\Delta\psi_N$ monitored on the sensor surface[55] at different [salt] with the exponential function of PEM thickness. Physically, the ES influence of the last PE layer gets screened by PEM. From the fit $\Delta\psi_N(x_m) \sim e^{-\kappa_m x_m}$ we extract the ionic strength inside PEMs being ∼1, ∼0.26, and ∼0.19 mM for the external salinities of 100, 10, and 1 mM, respectively; cf. Figure 4. The Debye lengths inside PEMs are then ∼9.5, ∼18.8, and ∼21.8 nm, correspondingly. These very low salinities inside PAH/PSS agree with the experimental data[59] validating small salinities used for model calculations in Figures 2 and 3.

This model is similar to the ES capacitor model[14] for potential oscillations on the sensor surface. The difference is that we neglect potential variations inside Si/SiO_2 structure and describe the exponential potential decay in the outer electrolyte. We assume extensive interpenetration of PE layers neglecting internal PEM structure. Such a "jelly-like" ES model of PEM was shown[14] to provide very similar results for the ES potential as compared to the more complex model with distinct/separated PE layers.

3. EFFECT OF PH ONTO POTENTIAL OSCILLATIONS

a. Charge Regulation. The measurements of $\psi_s(0)$ variations on the sensor surface can be performed experimentally without and with pH buffer (fixing the pH value, e.g., at 5.4 in ref 55). With the buffer, at moderate 0.1 M of NaCl the $\Delta\psi_N$ values observed are smaller in magnitude and decay more rapidly with the number of PE layers N. The PEM thickness for both cases is expected to be similar (unpublished). Thus, potential variations on the sensor originate *both* from direct ES influence of the outermost PE layer and from changes in pH and dissociation equilibrium at SiO_2−PEM interface. We present below a physical model for this effect.

In particular, in contrast to the model of section 2 with the sensor charge density being independent of its potential and bulk pH, the potentials of real SiO_2 surfaces were reported to decrease by ∼40 mV per pH unit, in the range from pH ∼2 to ∼7. The dissociation constant for SiO_2 surface groups of p$K_a \approx$ 5.7 was reported in ref 61, where the sensitivity of FED biosensors was investigated theoretically as a function of external parameters. Likewise, the charged state of weak PE chains gets altered upon PEM formation. For instance, for weak PAH chains, the apparent dissociation constant reflecting the chain protonation equilibrium was measured at ∼8.6.[62] In PEM, however, this bulk value might shift by 1−3 pH units to more alkaline region resulting in higher pK_a due to ES interactions with neighboring chains in PEM; see also refs 33,63.

Recently, a qualitative explanation for more pronounced and persistent potential oscillations without the pH-buffers was suggested based on pH-profile distribution inside PEMs.[64] It was argued that the enhancement in ES potential shifts detected might originate from the acid−base equilibrium on the sensor surface and in the first PAH layer. Namely, for PAH/PSS PEMs upon adsorption of PAH1 layer the protons are released from silicon dioxide chargeable groups, the pH value close to SiO_2−PEM interface gets reduced, the sensor surface thus becomes less charged, and its ES potential increases. This acts in the same direction as the direct potential rise accompanying PAH adsorption via the ES effect (see ref 14). Similarly, the PSS2 adsorption after the PAH1 layer can trigger an increase of pH in the PAH1 layer due to PAH protonation, the H+ concentration in PAH layer is reduced, and the sensor surface becomes more negatively charged. This results again in potential shifts in the same direction as coming from the ES influence of the PSS layer.

This explanation for enhancement of the sensor potential shifts upon PEM formation from pH unbuffered solutions is, however, inconsistent with the effect of Donnan equilibrium. The latter describes the Boltzmann-like populations of mobile ions in the regions with a given average ES potential.[65,66] Namely, for PAH/PSS PEMs the positive ions should

accumulate in PSS layers and anions should prefer PAH layers. Experiments on PAH/PSS PEMs[67] have indeed shown that PAH-terminated PEMs (with more positive ES potential in the structure that attracts anions) contain ~40 times more Br^- ions than PEMs terminated by a PSS layer (more negative ES potential repel anions from PEMs). Then, the H+ protons should be *expelled* from the first PAH layer, the pH value near SiO_2 surface will increase, giving rise to a more *negative* potential on SiO_2−PEM interface. This effect on the sensor potential is *opposite* to the direct ES influence of the PAH layer being adsorbed, as already mentioned.[50] The same explanation can be offered for adsorption of subsequent PAH layers which also give rise to an overall pH increase inside PEMs. This pH rise can be quantified using PAH-mediated potential increase on the sensor surface.

For instance, near an isolated negatively charged planar silica surface the positive mobile ions and protons are distributed according to ES potential $\psi(x) < 0$ as given by the Boltzmann law, $[H_+(x)] = [H_+(\infty)]\, e^{-\psi(x)}$. Here, $[H_+(\infty)]$ is the concentration of protons far from the interface, so that $pH = -\log_{10}[H_+(\infty)]$. Then, the actual $pH(x)$ value decreases toward the surface due to progressive accumulation of protons in the region of more negative potential,[68] namely, $pH(x) = -\log_{10}[H_+(x)] \approx pH + \psi(x)/2.3 < pH$. The charge state of ionizable groups on the SiO_2 surface can be rationalized via the Grahame equation[69] and dissociation constant Z of surface chargeable groups.[70] The Grahame equation couples the value of σ_s with ionic strength and surface potential; in the linear ES theory it is given by $-(\eta/S_S) = (\kappa\psi(0)/4\pi l_B)$. The fraction η of the charged surface groups is $\eta = 1/(1 + e^{-\psi(0)}10^{-(pH-pK_a)})$, where $pK_a = -\log_{10}Z$. Then, the final transcendental equation for the surface potential is $-1/(1 + e^{-\psi(0)}10^{-(pH-pK_a)}) = (S_s\kappa\psi(0)/4\pi l_B)$, where the $pH(x)$ decrease near the surface is accounted for.

This equation for $\psi(0)$ predicts that for electrolytes with a fixed ionic strength, with increase of the pH value the surface potential $\psi(0)$ becomes more negative and the surface charge grows from nearly neutral to fully charged surfaces. Also, at a fixed bulk pH value and with decreasing salt amount, the fraction of ionized groups decreases while the surface potential $\psi(0)$ becomes more negative, cf., the curves for different salinities in Figure 5. We can use these results to estimate the effect of adsorption of the PAH1 layer onto the sensor surface. In particular, the concentrations of mobile ions in PAH layers are known to be much lower than in bulk electrolyte, at least at a typical salt amount of 0.1 M. It means that the adsorption of the PAH1 layer dramatically reduces the [ion] near the sensor surface and thereby shifts the potential value down to −100 mV, as one can judge comparing the blue and red curves at large pH in Figure 5. This shift is pronounced upon formation of PAH/PSS PEMs on carbon nanotube transistor devices investigated in ref 71.

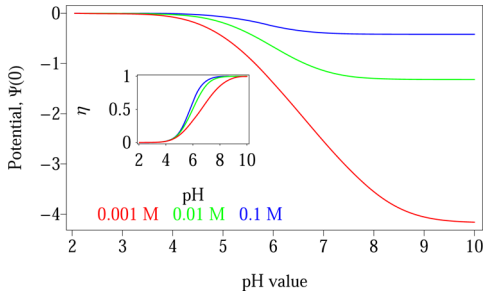

Figure 5. Dependence of ES surface potential $\psi(0)$ in dimensionless units (25 mV = 1) and the surface charged fraction η on the bulk pH for different values of the bulk ionic strength. The color coding and parameters are the same as in Figure 3; the experimental $pK_a = 5.7$[61] was used for the silicon dioxide surface.

b. Self-Consistent PE Adsorption and Surface Charge Regulation. As mentioned in the Introduction, typical sensor potential differences observed upon PAH/PSS adsorption are ~10−100 mV; see ref 55. The SiO_2 surface has $pH_{pzc} \approx 2$,[72] and thus its potential at pH = 7 reaches approximately −200 mV. The pH near the SiO_2 surface changes upon PAH1 adsorption and, to treat this self-consistently, we need to consider the Poisson−Boltzmann equation for $\psi(x)$ coupled to the polymer distribution $\phi(x)$ near the adsorbing surface. This set of coupled nonlinear differential equations is to be supplied with the boundary conditions for the surface charge density (dependent on [H+] near the surface). Then, one can get that[73−75] $\psi''(x) - \kappa^2 \sinh \psi(x) = -4\pi l_B p(\phi^2(x) - \phi_0^2 e^{\psi(x)})$, $b^2\phi''(x)/6 = \upsilon(\phi(x)^3 - \phi_0^2\phi(x)) + p\phi(x)\psi(x)$ with the conditions $\phi'(x) = 0$, $\psi'(0) = 4\pi l_B/S_s > 0$, $\psi'(x_{max}) = 0$, $\phi'(x_{max}) = 0$. Here, p is the PE charge fraction (PE is polycationic) and b is its Kuhn length. The distance x_{max} is the maximal separation from the surface up to which the ES potential $\psi(x)$ and polymer concentration $\phi^2(x)$ are to be computed. Note that the sum of the polymer charges and mobile electrolyte charges in the adsorbed layer compensate the surface charge density.

The numerical solution of this system of equations indicates that upon polycation adsorption on a negatively charged surface the mobile cations and H+ are *expelled* from the surface vicinity and the surface ES potential decreases in magnitude, as compared to the bare surface (not shown). Then, the pH value near the surface *increases* and due to charge regulation the SiO_2 surface becomes more *negatively charged*. Similarly to the Donnan effect discussed above, this self-consistent picture gives an *opposite* effect to the potential variations observed in the constant capacitance method upon PAH1 adsorption.[55] As the negative surface charges are compensated in experiments *both* by positive PE chains and by mobile cations, the decrease of the pH toward the surface due to accumulation of H+ can be weaker.

Local pH variations in PAH/PSS PEMs were measured through fluorescence of pH-sensitive dyes incorporated into the PAH1 layer.[68] The dye intensity increases with the buffer pH. Upon adsorption of PSS layers, the increase of dye intensity was detected indicating *larger* pH values in PAH1 for PSS-terminated PEMs. Thus, [H+] is smaller there, contrary to the expectation that more negative ES potentials inside PSS-terminated PEMs gather more protons. This is in agreement with our conclusions. It was also argued that the influence of the Donnan equilibrium is relatively weak for such PEM-related systems.[68] For PAH-terminated PEMs, the dye fluorescent intensity in the PAH1 layer was shown to decrease, respectively. These alternating charges of pH near the sensor surface are due to PEM permeability to protons,[68] which decreases with the number of PE layers N.

c. Linear vs Nonlinear Poisson−Boltzmann Models. Finally, we examine the effects of both charge regulation on the SiO_2 negatively charged surface and nonlinear Poisson−Boltzmann theory (applicable to arbitrary ES potentials). As we have seen above, the degree of dissociation α of surface ionizable groups depends on the pH value and ES surface

dx.doi.org/10.1021/jp502460v | J. Phys. Chem. B 2014, 118, 4552−4560

potential. This degree α should be found *self-consistently* via providing the corresponding boundary conditions for the full Poisson−Boltzmann equation, as described in ref 70. Positive mobile ions in solution (including protons) are distributed near the negative surface $\psi(0) < 0$ according to the Boltzmann distribution. For [H+] away from the surface we have $[H_+(x)] = [H_+(\infty)]\, e^{-\psi(x)}$. The pH value *decreases* toward the surface due to progressive accumulation of protons, $pH(x) \approx pH(\infty) + \psi(x)/2.3$; see the right panel in Figure 6. On charge-regulated

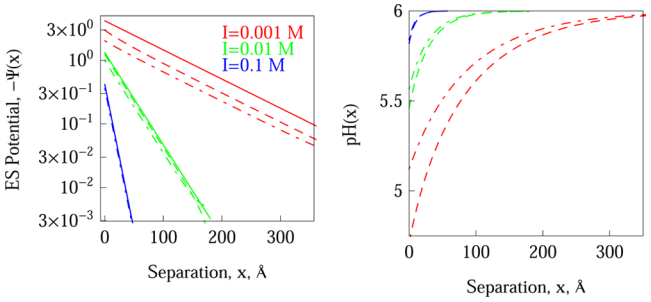

Figure 6. (Left) Magnitude of dimensionless ES potential $|\psi(x)|$ (25 mV is equal to 1) and (Right) $pH(x)$, both varying from a negatively charged interface. The computations are done for the nonlinear Poisson−Boltzmann model with (dot-dashed lines) and without the charge regulation (dashed lines). The "linear" result $\psi(x) = -4\pi l_B e^{-\kappa x}/(\kappa S_s)$ is shown as the solid lines. The color-coding for varying salinities is the same as in Figure 3. Parameters: $\varepsilon_m = 80$, $\sigma_{max} = -e_0/S_S = -e_0/2000$ Å^2, $pH(\infty) = 6$, i.e., $[H_+(\infty)] = 10^{-6}$ M, and $pK_a = 5$ (close to 5.7 reported for SiO_2 surfaces[61]).

surfaces, the degree of ionization of surface groups α is determined by their dissociation constant Z via $Z = [H_+(0)]\alpha/(1-\alpha)$. The ionization degree $\alpha(\psi(0)) = (Ze^{\psi(0)}/[H_+(\infty)])/(1 + Ze^{\psi(0)}/[H_+(\infty)])$ grows toward unity for more positive surface potentials and decreases to zero for negative ones. The nonlinear Poisson−Boltzmann equation for ES potential $\psi''(x) = \kappa^2 \sinh[\psi(x)]$ is supplied by the condition $\psi'(0) = 4\pi l_B \alpha/S_s$, where $\sigma_s = -e_0\alpha/S_s$. The value of $\psi(0)$ is adjusted in the numerical solution so that ES potential decays to zero far from the surface.

The numerical solution reveals that on charge-regulated surfaces the surface potentials are *smaller* in magnitude because the surface groups are not fully charged, $\alpha < 1$. The self-consistent α decreases in low-salt solutions. Namely, for the parameters of Figure 6 we obtain $\alpha \approx 0.57$ at 0.001 M, $\alpha \approx 0.79$ at 0.01 M, and $\alpha \approx 0.87$ at 0.1 M of simple salt. The maximal surface charge in Figure 6 corresponds to σ_s used in Figure 3. The decrease of pH toward the surface is therefore stronger for surfaces without charge regulation, cf., the dashed and dot-dashed curves in the right panel of Figure 6. We also observe that the linear Poisson−Boltzmann model overestimates the magnitude of the surface potential, particularly (as expected) in the low-salt limit when $|\psi(0)| \gg 25$ mV. Inspecting the magnitude of deviations of the linear vs nonlinear ES potentials presented in the left panel of Figure 6 for varying salinities, one can assess how much weaker the potential signals upon PEM formation obtained from the linear model in Figures 2 and 3 would be if a more accurate nonlinear ES model is implemented. The overall shape of zigzag potential oscillations remains similar in the nonlinear ES model (not shown).

4. CONCLUSIONS

The results obtained demonstrate the feasibility of FEDs for studying the effects induced by adsorption of charged macromolecules. The sensor response to PE adsorption is generated both by intrinsic charge of adsorbed molecules and by redistribution of ions within PEM structures. We have shown by theoretical modeling of PEMs that the sign and charge density of the terminating PE layer play the dominant role for the magnitude of signals detected on the sensor−PEM interface. We computed the distribution of the ES potential and potential variation on the sensor surface upon alternating PE deposition in PEM structures. We also examined the values of the Debye lengths inside PEMs at varying external salinities, the potential differences for linear vs nonlinear Poisson−Boltzmann models, and the implications of charge regulation on the adsorbing interface.

We have shown that as the ionic strength in electrolyte decreases, the amplitude of signals generated by sequential PE adsorption on the sensor surface grows progressively. This suggests that such low-salt buffers are most appropriate conditions not only for detection of highly charged PEs, as in the present paper, but also for monitoring adsorption of other charged biomolecules which are often much less charged (proteins, enzymes, DNA, etc.). The results predicted from the model are in qualitative agreement with experimental measurements.

A number of aspects of PEM formation beyond the scope of the current model remain to be exploited. The list includes several PEM structural parameters: the degree of PE layer interpenetration, the porosity of PE layers to H+ and larger ions, the pH profile throughout PEMs,[76] PEM roughness,[77] the degree of PE charge neutralization by cations trapped inside PEMs, the dielectric permittivity of PEMs, the level of PE hydration, and so forth.[78] The effects of external control parameters such as [salt] and pH buffers on structure and thickness of PE layers being formed, the deposition time of each PE layer, polymer molecular weight, the bulk polymer concentration, as well as the charge ratio of polycation to polyanion are nontrivial parameters to be included in future theoretical models of PEMs.

AUTHOR INFORMATION

Corresponding Author

*Email: a.cherstvy@gmail.com.

Notes

The authors declare no competing financial interest.

ACKNOWLEDGMENTS

The author acknowledges discussions with M. Weil (nee Abouzar) and A. Poghossian and financial support by the Deutsche Forschungsgemeinschaft (DFG Grant CH 707/5-1).

ABBREVIATIONS

PE, polyelectrolyte; PEM, polyelectrolyte multilayer; ES, electrostatic; FED, field-effect device; PAH, poly(allylamine hydrochloride); PSS, poly(sodium 4-styrenesulfonate); [salt], salt concentration

REFERENCES

(1) Daniels, J. S.; Pourmand, N. Label-Free Impedance Biosensors: Opportunities and Challenges. *Electroanalysis* **2007**, *19*, 1239−1257.

(2) Grieshaber, D.; MacKenzie, R.; Voros, J.; Reimhult, E. Electrochemical Biosensors - Sensor Principles and Architectures. *Sensors* **2008**, *8*, 1400−1458.
(3) Schöning, M. J.; Poghossian, A. Recent Advances in Biologically Sensitive Field-effect Transistors (BioFETs). *Analyst* **2002**, *127*, 1137−1151.
(4) Fritz, J.; Cooper, E. B.; Gaudet, S.; Sorger, P. K.; Manalis, S. R. Electronic Detection of DNA by its Intrinsic Molecular Charge. *Proc. Natl. Acad. Sci. U.S.A.* **2002**, *99*, 14142−14146.
(5) Uslu, F.; Ingebrandt, S.; Mayer, D.; Böcker-Meffert, S.; Odenthal, M.; Offenhäusser, A. Labelfree Fully Electronic Nucleic Acid Detection System Based on a Field-effect Transistor Device. *Biosens. Bioelectron.* **2004**, *19*, 1723−1731.
(6) Pouthas, F.; Gentil, C.; Cote, D.; Bockelmann, U. DNA Detection on Transistor Arrays Following Mutation-Specific Enzymatic Amplification. *Appl. Phys. Lett.* **2004**, *84*, 1594−1596.
(7) Sakata, T.; Miyahara, Y. DNA Sequencing Based on Intrinsic Molecular Charges. *Angew. Chem., Int. Ed.* **2006**, *45*, 2225−2228.
(8) Estrela, P.; Migliorato, P.; Takiguchi, H.; Fukushima, H.; Nebashi, S. Electrical Detection of Biomolecular Interactions with Metal−Insulator−Semiconductor Diodes. *Biosens. Bioelectron.* **2005**, *20*, 1580−1586.
(9) Lud, S. Q.; et al. Field Effect of Screened Charges: Electrical Detection of Peptides and Proteins by a Thin-film Resistor. *ChemPhysChem* **2006**, *7*, 379−384.
(10) Cherstvy, A. G. Detection of DNA Hybridization by Field-effect DNA-based Biosensors: Mechanisms of Signal Generation and Open Questions. *Biosens. Bioelectron.* **2013**, *46*, 162−170.
(11) Bergveld, P. A Critical Evaluation of Direct Electrical Protein Detection Methods. *Biosens. Bioelectron.* **1991**, *6*, 55−72.
(12) Poghossian, A.; Cherstvy, A. G.; Ingebrandt, S.; Offenhäusser, A.; Schöning, M. J. Possibilities and Limitations of Label-free Detection of DNA Hybridization with Field-effect-based Devices. *Sens. Actuators, B* **2005**, *111−112*, 470−480.
(13) Poghossian, A.; et al. Field-effect Sensors for Monitoring the Layer-by-layer Adsorption of Charged Macromolecules. *Sens. Actuators, B* **2006**, *118*, 163−170.
(14) Neff, P. A.; Naji, A.; Ecker, C.; Nickel, B.; von Klitzing, R.; Bausch, A. R. Electrical Detection of Self-Assembled Polyelectrolyte Multilayers by a Thin Film Resistor. *Macromolecules* **2006**, *39*, 463−466.
(15) Decher, G.; Hong, J. D.; Schmitt, J. Buildup of Ultrathin Multilayer Films by a Self-assembly Process: III. Consecutively Alternating Adsorption of Anionic and Cationic Polyelectrolytes on Charged Surfaces. *Thin Solid Films* **1992**, *210*, 831−835.
(16) Decher, G. Fuzzy Nanoassemblies: Toward Layered Polymeric Multicomposites. *Science* **1997**, *277*, 1232−1237.
(17) Lösche, M.; Schmitt, J.; Decher, G.; Bouwman, W. G.; Kjaer, K. Detailed Structure of Molecularly Thin Polyelectrolyte Multilayer Films on Solid Substrates as Revealed by Neutron Reflectometry. *Macromolecules* **1998**, *31*, 8893−8906.
(18) Schoenhoff, M. Self-assembled Polyelectrolyte Multilayers. *Curr. Opin. Colloid Interface Sci.* **2003**, *8*, 86−95.
(19) von Klitzing, R. Internal Structure of Polyelectrolyte Multilayer Assemblies. *Phys. Chem. Chem. Phys.* **2006**, *8*, 5012−5033.
(20) Bieker, P.; Schoenhoff, M. Linear and Exponential Growth Regimes of Multilayers of Weak Polyelectrolytes in Dependence on pH. *Macromolecules* **2010**, *43*, 5052−5059.
(21) Hammond, P. T. Recent Explorations in Electrostatic Multilayer Thin Film Assembly. *Curr. Opin. Colloid Interface Sci.* **1999**, *4*, 430−442.
(22) Hammond, P. T. Form and Function in Multilayer Assembly: New Applications at the Nanoscale. *Adv. Mater.* **2004**, *16*, 1271−1293.
(23) Harries, D.; May, S.; Ben-Shaul, A. Counterion Release in Membrane−Biopolymer Interactions. *Soft Matter* **2013**, *9*, 9268−9284.
(24) Cherstvy, A. G.; Petrov, E. P. Modeling DNA Condensation on Freestanding Cationic Lipid Membranes. *Phys. Chem. Chem. Phys.* **2014**, *16*, 2020−2037.
(25) Schlenoff, J. B.; Hiep, L.; Ming, L. Charge and Mass Balance in Polyelectrolyte Multilayers. *J. Am. Chem. Soc.* **1998**, *120*, 7626−7634.
(26) Schlenoff, J. B.; Dubas, S. T. Mechanism of Polyelectrolyte Multilayer Growth: Charge Overcompensation and Distribution. *Macromolecules* **2001**, *34*, 592−598.
(27) Shiratori, S. S.; Rubner, M. F. pH-Dependent Thickness Behavior of Sequentially Adsorbed Layers of Weak Polyelectrolytes. *Macromolecules* **2000**, *33*, 4213−4219.
(28) Yoo, D.; Shiratori, S. S.; Rubner, M. F. Controlling Bilayer Composition and Surface Wettability of Sequentially Adsorbed Multilayers of Weak Polyelectrolytes. *Macromolecules* **1998**, *31*, 4309−4318.
(29) Choi, J.; Rubner, M. F. Influence of the Degree of Ionization on Weak Polyelectrolyte Multilayer Assembly. *Macromolecules* **2005**, *38*, 116−124.
(30) Steitz, R.; Leiner, V.; Siebrecht, R.; von Klitzing, R. Influence of the Ionic Strength on the Structure of Polyelectrolyte Films at the Solid/Liquid Interface. *Colloids Surf. A* **2000**, *163*, 63−70.
(31) Lourenco, J. M. C.; Ribeiro, P. A.; Botelho do Rego, A. M.; Raposo, M. Counterions in Layer-by-layer Films—Influence of the Drying Process. *J. Colloid Interface Sci.* **2007**, *313*, 26−33.
(32) Burke, S. E.; Barrett, C. J. Acid-Base Equilibria of Polyelectrolytes in Multilayer Thin Films. *Langmuir* **2003**, *19*, 3297−3303.
(33) Petrov, A. I.; Petrov, A. I.; Antipov, A. A.; Sukhorukov, G. B. Base-Acid Equilibria in Polyelectrolyte Systems: From Weak Polyelectrolytes to Interpolyelectrolyte Complexes and Multilayered Polyelectrolyte Shells. *Macromolecules* **2003**, *36*, 10079−10086.
(34) Schoenhoff, M.; et al. Hydration and Internal Properties of Polyelectrolyte Multilayers. *Colloids Surf. A* **2007**, *303*, 14−29.
(35) Wong, J. E.; Zastrow, H.; Jaeger, W.; von Klitzing, R. Specific Ion versus Electrostatic Effects on the Construction of Polyelectrolyte Multilayers. *Langmuir* **2009**, *25*, 14061−14070.
(36) Joseph, N.; Ahmadiannamini, P.; Hoogenboom, R.; Vankelecom, Ivo. F. J. Layer-by-Layer Preparation of Polyelectrolyte Multilayer Membranes for Separation. *Polym. Chem.* **2014**, *5*, 1817−1831.
(37) Bertrand, P.; Jonas, A.; Laschewsky, A.; Legras, R. Ultrathin Polymer Coatings by Complexation of Polyelectrolytes at Interfaces: Suitable Materials, Structure and Properties. *Macromol. Rapid Commun.* **2000**, *21*, 319−348.
(38) DeRocher, J. P.; Mao, P.; Kim, J. Y.; Han, J.; Rubner, M. F.; Cohen, R. E. Layer-by-Layer Deposition of All-Nanoparticle Multilayers in Confined Geometries. *ACS Appl. Mater. Interfaces* **2012**, *4*, 391−396.
(39) Gauczinski, J.; Liu, Z.; Zhang, Xi; Schönhoff, M. Mechanism of Surface Molecular Imprinting in Polyelectrolyte Multilayers. *Langmuir* **2010**, *26*, 10122−10128.
(40) Parveen, N.; Schönhoff, M. Swelling and Stability of Polyelectrolyte Multilayers in Ionic Liquid Solutions. *Macromolecules* **2013**, *46*, 7880−7888.
(41) Castelnovo, M.; Joanny, J. F. Formation of Polyelectrolyte Multilayers. *Langmuir* **2000**, *16*, 7524−7532.
(42) Netz, R. R.; Joanny, J. F. Adsorption of Semiflexible Polyelectrolytes on Charged Planar Surfaces: Charge Compensation, Charge Reversal, and Multilayer Formation. *Macromolecules* **1999**, *32*, 9013−9025.
(43) Park, S. Y.; Rubner, M. F.; Mayes, A. M. Free Energy Model for Layer-by-Layer Processing of Polyelectrolyte Multilayer Films. *Langmuir* **2002**, *18*, 9600−9604.
(44) Szilagyi, I.; et al. Polyelectrolyte Adsorption, Interparticle Forces, and Colloidal Aggregation. *Soft Matter* **2014**, *10*, 2479−2502.
(45) Dobrynin, A. V.; Rubinstein, M. Theory of Polyelectrolytes in Solutions and at Surfaces. *Progr. Polym. Phys.* **2005**, *30*, 1049−1118.
(46) Shafir, A.; Andelman, D. Polyelectrolyte Multilayer Formation: Electrostatics and Short-Range Interactions. *Eur. Phys. J. E* **2006**, *19*, 155−162.
(47) Patel, P. A.; Jeon, J.; Mather, P. T.; Dobrynin, A. V. Molecular Dynamics Simulations of Layer-by-Layer Assembly of Polyelectrolytes

at Charged Surfaces: Effects of Chain Degree of Polymerization and Fraction of Charged Monomers. *Langmuir* **2005**, *21*, 6113−6122.
(48) Carrillo, J. M. Y.; Dobrynin, A. V. Molecular Dynamics Simulations of Polyelectrolyte Adsorption. *Langmuir* **2007**, *23*, 2472−2482.
(49) Carrillo, J. M. Y.; Dobrynin, A. V. Layer-by-Layer Assembly of Polyelectrolyte Chains and Nanoparticles on Nanoporous Substrates: Molecular Dynamics Simulations. *Langmuir* **2012**, *28*, 1531−1538.
(50) Wunderlich, B. K.; Neff, P. A.; Bausch, A. R. Mechanism and Sensitivity of the Intrinsic Charge Detection of Biomolecular Interactions by Field Effect Devices. *Appl. Phys. Lett.* **2007**, *91*, 083904.
(51) Park, S.; Barrett, C.; Rubner, M.; Mayes, A. Anomalous Adsorption of Polyelectrolyte Layers. *Macromolecules* **2001**, *34*, 3384−3388.
(52) Winkler, R. G.; Cherstvy, A. G. Strong and Weak Polyelectrolyte Adsorption onto Oppositely Charged Curved Surfaces. *Adv. Polym. Sci.* **2014**, *255*, 1−56.
(53) Cherstvy, A. G.; Winkler, R. G. Polyelectrolyte Adsorption onto Oppositely Charged Interfaces: Image-Charge Repulsion and Surface Curvature. *J. Phys. Chem. B* **2012**, *116*, 9838−9845.
(54) Cherstvy, A. G.; Winkler, R. G. Strong and weak adsorptions of polyelectrolyte chains onto oppositely charged spheres. *J. Chem. Phys.* **2006**, *125*, 064904.
(55) Poghossian, A.; Weil, M.; Cherstvy, A. G.; Schoning, M. J. Electrical Monitoring of Polyelectrolyte Multilayer Formation by Means of Capacitive Field-effect Devices. *Anal. Bioanal. Chem.* **2013**, *405*, 6425−6436.
(56) Abouzar, M. H. Detection of Molecular Interactions using Field-Effect-based Capacitive Devices; PhD Thesis; Humboldt University of Berlin, 2011.
(57) Weil, M. et al., unpublished results.
(58) The potential shifts in the buffered solutions are smaller and also decay faster with the number of PE layers. The latter is likely to originate from ions' redistribution in PEMs. Both the intrinsic PE charge and changes in ion concentrations contribute to the measured sensor signal. For PE adsorption from pH-buffered solutions, the local pH changes in PEMs are suppressed and the signals are dominated by the direct ES influence of the terminating PE layer.
(59) Neff, P. A.; Wunderlich, B. K.; v. Klitzing, R.; Bausch, A. R. Formation and Dielectric Properties of Polyelectrolyte Multilayers Studied by a Silicon-on-Insulator Based Thin Film Resistor. *Langmuir* **2007**, *23*, 4048−4052.
(60) Cherstvy, A. G. Electrostatics of DNA Complexes with Cationic Lipid Membranes. *J. Phys. Chem. B* **2007**, *111*, 7914−7927.
(61) McKinnon, W. R.; Landheer, D.; Aers, G. Sensitivity of Field-Effect Biosensors to Charge, *p*H, and Ion Concentration in a Membrane Model. *J. Appl. Phys.* **2009**, *104*, 124701.
(62) Mauser, T.; Déjugnat, C.; Sukhorukov, G. B. Reversible pH-Dependent Properties of Multilayer Microcapsules Made of Weak Polyelectrolytes. *Macromol. Rapid Commun.* **2004**, *25*, 1781−1785.
(63) Rmaile, H. H.; Schlenoff, J. B. Internal pKa's in Polyelectrolyte Multilayers: Coupling Protons and Salt. *Langmuir* **2002**, *18*, 8263−8265.
(64) Schöning, M. J.; Abouzar, M. H.; Poghossian, A. pH and Ion Sensitivity of a Field-effect EIS (Electrolyte-Insulator-Semiconductor) Sensor Covered with Polyelectrolyte Layers. *J. Solid State Electrochem.* **2009**, *13*, 115−122.
(65) Deserno, M.; von Grünberg, H. H. Osmotic Pressure of Charged Colloidal Suspensions: A Unified Approach to Linearized Poisson-Boltzmann Theory. *Phys. Rev. E* **2002**, *66*, 011401 and references cited therein.
(66) Cherstvy, A. G.; Kornyshev, A. A. DNA Melting in Aggregates: Impeded or Facilitated? *J. Phys. Chem. B* **2005**, *109*, 13024−13029.
(67) Schollmeyer, H.; et al. Ion Distribution in Polyelectrolyte Multilayers with Standing-Wave X-ray Fluorescence. *J. Phys. Chem. B* **2007**, *111*, 4036−4042.
(68) von Klitzing, R.; Möhwald, H. Proton Concentration Profile in Ultrathin Polyelectrolyte Films. *Langmuir* **1995**, *11*, 3554−3559.
(69) Israelachvili, J. *Intermolecular and Surface Forces*; Academic Press: London, 1992.
(70) Ninham, B. W.; Parsegian, V. A. Electrostatic Potential between Surfaces Bearing Ionizable Groups in Ionic Equilibrium with Physiologic Saline Solution. *J. Theor. Biol.* **1971**, *31*, 405−428.
(71) Artyukhin, A. B.; et al. Controlled Electrostatic Gating of Carbon Nanotube FET devices. *Nano Lett.* **2006**, *6*, 2080−2085.
(72) Kosmulski, M. in *Encyclopedia of Surface and Colloid Science*, 2nd ed.; Somasundaran, P., Ed.; CRC Press, 2006; p 1857.
(73) Borukhov, I.; Andelman, D.; Orland, H. Scaling Laws of Polyelectrolyte Adsorption. *Macromolecules* **1998**, *31*, 1665−1671.
(74) Borukhov, I.; Andelman, D.; Orland, H. Effect of Polyelectrolyte Adsorption on Intercolloidal Forces. *J. Phys. Chem. B* **1999**, *103*, 5042−5057.
(75) Netz, R. R.; Andelman, D. Polyelectrolytes in Solution and at Surfaces, in *Encyclopedia of Electrochemistry*; Bard, A. J., Stratmann, M., Gileadi, E., Urbakh, M., Eds.; Wiley, 2002; Vol. *1*, p 282.
(76) It is relevant for weak PEs such as PAH, which are almost fully ionized at pH = 2.5−6.5, while loose protons at pH > 7.0. The shift of pK_a of PAH can reach several units in some PEMs. The fundamental quantity is PAH protonation vs separation to SiO_2 surface and distance from the last PE layer. Also note that in the proximity of a negative SiO_2, the adsorption of PAH1 layer leads to a depletion of protons and larger pH. The deposition of PSS2 layer, per contra, attracts more protons into this layer and thus reduces the apparent pH there. To what extent this influences the pH near the sensor surface as more PE layers are getting deposited, crucially depends on the porosity of a given PEM.
(77) The typical layer thickness at 0.1 M NaCl, pH = 5.4, and for the molecular weight of PSS/PAH used of 70 000 was ca. 2 nm.[55] The surface roughness of PEMs obtained was shown to increase with the number of adsorbed layers, from 2.4 nm for PSS2 layer to 6 nm for PAH11.[55] Note that this more irregular mixing of PEs in the terminating layer can per se result in some smearing out of ES potential oscillations after a large number of PE layers deposited.
(78) Dodoo, S. Structure and Swelling Behavior of Polyelectrolyte Multilayers; PhD Thesis; Technical University of Berlin, 2011.